Naval Ocean Systems Center
San Diego, CA 92152-5000

4

Technical Document 1355
September 1988

Infrared Sea-Radiance Modeling Using Lowtran 6

F. G. Wollenweber

NAVAL OCEAN SYSTEMS CENTER

San Diego, California 92152-5000

E. G. SCHWEIZER, CAPT, USN
Commander

R. M. HILLYER
Technical Director

ADMINISTRATIVE INFORMATION

This task was performed by F.G. Wollenweber during his tour as a visiting Scientist in the Ocean and Atmospheric Sciences Division at the Naval Ocean Systems Center. The project was funded by the Office of Naval Technology under program element 62435N.

Released by
H.V. Hitney, Head
Tropospheric Branch

Under authority of
J.H. Richter, Head
Ocean and Atmospheric
Sciences Division

PK

UNCLASSIFIED
SECURITY CLASSIFICATION OF THIS PAGE

REPORT DOCUMENTATION PAGE

1a. REPORT SECURITY CLASSIFICATION UNCLASSIFIED	1b. RESTRICTIVE MARKINGS
2a. SECURITY CLASSIFICATION AUTHORITY	3. DISTRIBUTION/AVAILABILITY OF REPORT Approved for public release; distribution is unlimited.
2b. DECLASSIFICATION/DOWNGRADING SCHEDULE	
4. PERFORMING ORGANIZATION REPORT NUMBER(S) NOSC Technical Document 1355	5. MONITORING ORGANIZATION REPORT NUMBER(S)
6a. NAME OF PERFORMING ORGANIZATION Naval Ocean Systems Center 6b. OFFICE SYMBOL (if applicable) NOSC Code 543	7a. NAME OF MONITORING ORGANIZATION Naval Ocean Systems Center
6c. ADDRESS (City, State and ZIP Code) San Diego, California 92152-5000	7b. ADDRESS (City, State and ZIP Code) San Diego, California 92152-5000
8a. NAME OF FUNDING/SPONSORING ORGANIZATION Office of Naval Technology 8b. OFFICE SYMBOL (if applicable) Code 21	9. PROCUREMENT INSTRUMENT IDENTIFICATION NUMBER
8c. ADDRESS (City, State and ZIP Code) Arlington, VA 22217-5000	10. SOURCE OF FUNDING NUMBERS PROGRAM ELEMENT NO.: 62435N PROJECT NO.: RU35G80 TASK NO.: AGENCY ACCESSION NO.: DN888 715

11. TITLE (include Security Classification)
INFRARED SEA-RADIANCE MODELING USING LOWTRAN 6

12. PERSONAL AUTHOR(S)
F.G. Wollenweber

13a. TYPE OF REPORT	13b. TIME COVERED	14. DATE OF REPORT (Year, Month, Day)	15. PAGE COUNT
Final	FROM TO	September 1988	25

16. SUPPLEMENTARY NOTATION

17. COSATI CODES			18. SUBJECT TERMS (Continue on reverse if necessary and identify by block number)
FIELD	GROUP	SUB-GROUP	sea state, wave shadowing, emissivity, reflectivity, radiance

19. ABSTRACT (Continue on reverse if necessary and identify by block number)

A model, based on the Cox-Monk wave-slope statistic and the LOWTRAN 6 radiation model, describes the behavior of the sea as an infrared (IR) background. The model addresses atmospheric refraction, aerosol absorption and scattering, molecular scattering, emission, and absorption. Comparisons with measurements of a calibrated thermal-imaging system showed good agreement.

20. DISTRIBUTION/AVAILABILITY OF ABSTRACT	21. ABSTRACT SECURITY CLASSIFICATION
☐ UNCLASSIFIED/UNLIMITED ☒ SAME AS RPT ☐ DTIC USERS	UNCLASSIFIED

22a. NAME OF RESPONSIBLE PERSON	22b. TELEPHONE (include Area Code)	22c. OFFICE SYMBOL
H.G. Hughes	619-553-1418	Code 543

DD FORM 1473, 84 JAN

83 APR EDITION MAY BE USED UNTIL EXHAUSTED
ALL OTHER EDITIONS ARE OBSOLETE

UNCLASSIFIED
SECURITY CLASSIFICATION OF THIS PAGE

SUMMARY

OBJECTIVE

Describe behavior of the sea as an infrared background.

RESULTS

In three cases, the suggested model was able to predict sea-radiance values.

RECOMMENDATIONS

Demonstrate how often a simple sea-state model can be used and under which circumstances it fails.

Address the height requirement at which the temperature and humidity profiles need to be measured to obtain better agreement between measured and calculated radiances.

Determine the maximum number of zenith angles required to represent the measured radiances.

Investigate the validity of a single frequency-dependent emissivity and reflectivity.

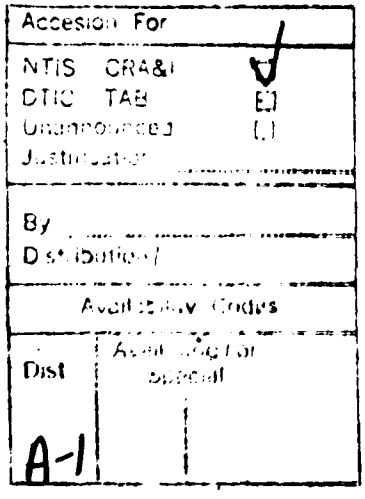

CONTENTS

1.0 INTRODUCTION

A thorough understanding of target backgrounds is necessary to describe the performance of passive infrared (IR) surveillance systems. A model has been developed based on the well known Cox-Munk wave-slope statistics (Cox and Munk, 1954) and the LOWTRAN 6 optical propagation code (Kneizys et al., 1983), to predict the behaviour of sea radiance backgrounds. Similar approaches have been published in the past, but they neglected important processes. Saunders (1968) modeled sea radiance but neglected the path radiance between the sensor and the sea surface and also aerosol effects. Sidran (1981), as well as Schwartz and Hon (1986) studied only the effects of sea-surface roughness on emissivity. Wilf and Manor (1984) addressed the path radiance between the sensor and the sea in a simplified way by neglecting aerosols. The model presented here is an improvement over earlier attempts since it addresses the effects of refraction and molecular absorption and emission, as well as the aerosol effects, which are important in determining the path radiance. The reflection geometry and the wave-slope distribution determine those portions of the sky that reflect energy into the line-of-sight of the receiving system. A provision is included for determining the effects of wave shadowing. The surface reflectivity and emissivity are calculated using the complex index of refraction of sea water in Fresnel's formulas. The model's ability to describe the sea and sky radiances for zenith angles close to the horizon is demonstrated by comparing calculated radiances using radiosonde soundings of the atmosphere with measurements of the 8- to 12-μm radiances using a calibrated thermal-imaging system.

2.0 THEORY

2.1 BASIC IDEAS

A IR system looking down at the sea surface receives energy from different sources. The air between sensor and sea surface emits and scatters radiation into the line-of-sight of the system. The sea surface reflects parts of the sky's radiance and emits with the water temperature T_w. The emissivity and reflectivity of salt water can be determined by Fresnel's formulas. A frequency-dependent complex index of refraction has to be used. Reflected sky radiance, as well as the thermal emission of the sea, have to be multiplied by the transmissivity τ, of the path between sensor and sea surface to address loss of energy due to scattering and absorption. Figure 1 shows the geometry of a reflection due to waves with an angular tilt of α in wind direction and β perpendicular to the wind direction. The curvature of the path was a result of atmospheric refraction.

Equation (1) determines the radiance received by the sensor and contains all the above mentioned contributions.

$$S(\Theta,k) = \int_{\tau_a(S_1)}^{\tau_a(o)} \tau_s(\tau_a)\ (1/\pi) BB(k,T_a(\tau_a))\ d\tau_a \qquad (1)$$

$$+\ \tau(s_1)\ R(\Omega,k) \int_{\tau_a(S_1)}^{\tau_a(S_\infty)} \tau_s(\tau_a)\ (1/\pi) BB(k,T_a(\tau_a))\ d\tau_a$$

$$+\ \tau(s_1)\ (1 - R(\Omega,k))\ (1/\pi) BB(k,T_w)\ .$$

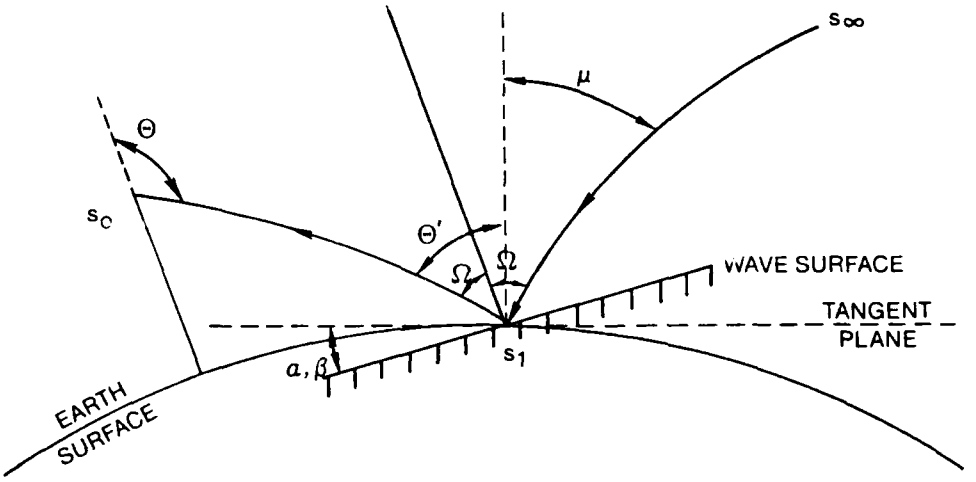

Figure 1. The geometry of a reflection at a wave is shown. The sensor zenith angle Θ is modified by atmospheric refraction resulting in an zenith angle Θ. The reflection angle Ω and the zenith angle μ from where radiance is reflected in the sensor line-of-sight are defined by the wave slopes α, β, and the angle Θ.

To evaluate equation (1), determine the transmission the optical path s, and the reflectivity R. The LOWTRAN 6 model is used to determine these values numerically. The actual optical path is controlled by the wave tilts S_x and S_y ($S_x = \tan \alpha$, $S_y = \tan \beta$), the sensor zenith angle Θ, and refractivity effects (*i.e., the vertical distribution* of temperature T_a, pressure (p), and relative humidity (RH)). Instead of momentary values of radiance, we are looking at spacial averages. The statistical distribution of wave tilts, together with the reflection geometry, determine the statistical distribution of zenith angles from radiance reflected into the observer line-of-sight. The average radiance is calculated by integrating over all zenith angles (equation 2)).

$$\bar{S}(\Theta,k) = \int_{\tau_a(S_0)}^{\tau_a(S_1)} \tau_s(\tau_a)\ (1/\pi)BB(k,T_a(\tau_a))\ d\tau_a \qquad (2)$$

$$+\ \tau(s_1) \int_{\mu=o}^{\mu=\text{horizon}} P(\mu)\ R(\Omega(\mu),k) \int_{\tau_a(S_1)}^{\tau_a(S_\infty)} \tau_s(\tau_a)\ (1/\pi)BB(k,T_a)\ d\tau_a\ d\mu$$

$$+\ \tau(s_1) \int_{\mu=o}^{\mu=\text{horizon}} P(\mu)\ (1 - R(\Omega(\mu),k))\ 1/\pi BB(k,T_w)\ d\mu$$

The wave-slope distribution necessary for these calculations has to be obtained from a sea-state model.

2.2 SEA-STATE MODEL

The Cox-Munk statistics were used to describe the wave tilts. The probability density function of wave tilts for a wind-driven sea was given by a Gram Charlier series. The coefficients were determined experimentally by Cox and Munk. A two-dimensional gaussian distribution has been used in this paper. Equation (3) shows the gaussian function together with the equations to determine the variances σ_x^2, σ_y^2 (x pointing downwind, y crosswind) of the wave slopes as functions of the windspeed (WS) (in m/s).

$$P(S_x, S_y) = 1/(2\pi\sigma_x\sigma_y)\ \mathrm{EXP}\,(0.5(S_x^2/\sigma_x^2 + S_y^2/\sigma_y^2))$$

$$\sigma_x^2 = 0.003 + 1.92\ 10^{-3}\ \mathrm{WS}$$

$$\sigma_y^2 = 3.16\ 10^{-3}\ \mathrm{WS}\ . \qquad (3)$$

One perspective of this investigation was to study how well a simple sea-state model corresponds with measured radiances. Different authors (Schwartz and Hon, 1986; Wu, 1972) showed that the Cox-Munk model underestimated the total variance of the wave slopes. Future work should investigate the influence of different relationships between the variances of wave slopes and windspeed, or other versions of a sea-state model.

2.3 GEOMETRY

Two different coordinate systems were used. The wind oriented system with its x-axis pointing downwind, the z-axis vertically upward, and the y-axis perpendicular to x and z so that a right-handed system was formed. In the wave-oriented system the x'-axis was within the wave surface pointing downwind. The z'-axis is normal to the wave surface and the y'-axis is perpendicular to x' and z' so that, again, a righthanded system was formed. The transition from one system to the other was possible through the use of the wave slopes S_x, S_y given in the wind-oriented system. By calculating the coordinate transforms between both systems, it was possible to derive the zenith angle μ (for those portions of the sky from where radiance is reflected into the line-of-sight) and the reflection angle Ω (equation (4)).

$$\cos\,\mu = 2S_x/A\,\cos\,\Theta'\,\cos\,\Phi + 2S_y\,A\,\cos\,\Theta'\,\cos\,\Phi \quad B\,A\,\sin\,\Theta'$$

$$\cos\,\Omega = S_x/A\,\cos\,\Theta'\,\cos\,\Phi + S_y\,A\,\cos\,\Theta'\,\cos\,\Phi + 1\,A\,\sin\,\Theta'$$

$$A = S_x^2 + S_y^2 + 1$$

$$B = S_x^2 + S_y^2 + 1\ . \qquad (4)$$

2.4 SHADOWING OF WAVES

For a given configuration of sensor zenith angle and wave slope, a certain percentage P_o of waves were hidden behind other waves. Thus, for this percentage of cases the reflected sky radiance did not come from the zenith angle that results from the geometry, but from other zenith angles. In contrast to another paper (Saunders, 1968), it is assumed that the radiance reflected from those zenith angles also contributed to the received radiance of the sensor.

In cases where shadowing must occur ($\Theta > 90°$ and $\Omega > 90°$), it is assumed that the radiance was reflected by the other side of the same wave. Equation (5) states zenith and reflection angle for those cases.

$$\cos \mu = -2S_x/A \cos \Theta' \cos \Phi - 2S_y/A \cos \Theta' \cos \Phi - B/A \sin \Theta' \text{ and} \quad (5a)$$

$$\cos \Omega = -S_x/A \cos \Theta' \cos \Phi - S_y/A \cos \Theta' \cos \Phi + 1/A \sin \Theta' \quad (5b)$$

$$A = S_x^2 + S_y^2 + 1$$

$$B = S_x^2 + S_y^2 - 1$$

In cases of multiple reflection as well as other shadowing events, it is assumed that the shadowed optical path hits another part of a normally distributed sea surface. This situation is described by the zenith-angle distribution already calculated. The probability for shadowing is distributed over the zenith angles according to the distribution function (Appendix 1).

2.5 REFLECTIVITY AND EMISSIVITY OF SEA WATER

The reflectivity (and emissivity) of water as a function of the reflection angle Ω and the complex index of refraction (mr, mi) is given by Fresnel's equations (6), (Stratton, 1941).

$$U^2 = 0.5(m_r^2 - m_i^2 - \sin^2\Omega + ((m_r^2 - m_i^2 - \sin^2\Omega)^2 + 4m_r^2m_i^2)^{0.5})$$

$$V^2 = 0.5(-(m_r^2 - m_i^2 - \sin^2\Omega) + ((m_r^2 - m_i^2 - \sin^2\Omega)^2 + 4m_r^2m_i^2)^{0.5})$$

$$C = (\cos \Omega - U)^2 + V^2$$

$$D = (\cos \Omega + U)^2 + V^2 \quad (6)$$

$$E = ((m_r^2 - m_i^2) \cos \Omega - U)^2 + (2m_rm_i\cos \Omega - V)^2$$

$$F = ((m_r^2 - m_i^2) \cos \Omega + U)^2 + (2m_rm_i\cos \Omega + V)^2$$

$$R_1^2 = C/D$$

$$R_2^2 = E/F$$

The reflectivity is given by equation (7).

$$R(\Omega,k) = 0.5 (R_1^2 + R_2^2) \quad (7)$$

For each wave number k, the complex index of refraction was determined. The values used were taken from Querry et al. (1977) and (Hale and Querry (1973)). Figure 2 shows the real and imaginary part of the refractivity.

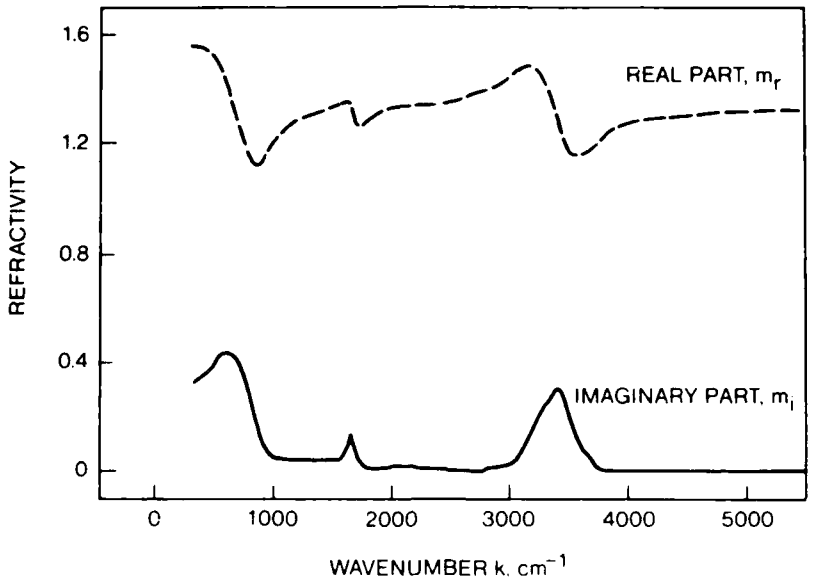

Figure 2. Real and imaginary parts m_r, m_i of refractivity as a function of wavenumber k.

A study of the dependence of reflectivity and emissivity on frequency showed, that in the 8- to 12-μm region the variability of these parameters is less than 5 percent. In terms of radiation temperature, the changes in emissivity and reflectivity could result in deviations of radiation temperature of about one degree. Since the effects of emissivity and reflectivity are counteracting, it is not clear what the overall effect would be. A closer look at this problem is necessary because it largely influences the computation time of the model.

2.6 NUMERICAL EVALUATION OF THE EQUATIONS

Equation (2) cannot be solved analytically and the integration must be approximated numerically. The reflection angles and zenith angles must be calculated with equations (3) and (4) for a given sensor zenith angle. The wave slopes are taken out of the intervals $-3\sigma_x < S_x < 3\sigma_x$, $-3\sigma_y < S_y < \sigma_y$ with an increment DS. The sky radiance for the different zenith angles is calculated by LOWTRAN 6. To limit the number of calculations, the zenith-angles are divided into classes. The results presented here were achieved with a maximum value of 30 different zenith-angle classes. The number of classes was further reduced by the criterion that each class should contain at least 10 percent of the probability. If a class does not exceed this value, it will be added to the next class and exceed the limit. For each zenith-angle class i, the average zenith angle $\mu(i)$, the probability of this class P(i) and the average reflection angle $\Omega(i)$ is calculated in equations 8, 9, and 10.

$$P(i) = \sum_{\mu} P(\mu) \ , \tag{8}$$

$$\mu(i) = \sum_{\mu} \mu P(\mu)/P(i) \ , \text{ and} \tag{9}$$

$$\Omega(i) = \sum_{\mu} \Omega(\mu) P(\mu)/P(i) \ . \tag{10}$$

For the average zenith angle, the sky radiance was calculated by LOWTRAN 6. This radiance was multiplied with the reflectivity for this zenith angle class R(i) and with the probability P(i). Subsequently, the values of all zenith angle classes were added. The emitted radiance of the ocean was accounted for by an averaged frequency-dependent emissivity EMIS. EMIS is calculated as an weighted average over all zenith angle classes (equation (11)).

$$EMIS = \Sigma P(i)_i (1 - R(\Omega(i), k)) / \Sigma P(i)_i \quad . \tag{11}$$

The radiance emitted by the ocean and the sum of the reflected sky radiances were multiplied by the transmissivity between sensor and ocean surface to account for attenuation along the path, then added to the emission of the air between the sensor and ocean surface to obtain the total radiance.

To accomplish all the different functions, several subroutines had to be added to the LOWTRAN 6 code.

3.0 PROGRAM CHANGES IN LOWTRAN 6

3.1 PROGRAM STRUCTURE

Figure 3 shows the structure of the LOWTRAN 6 main program together with different subprograms. The structure of the subroutine GEO is shown in figure 4. The subroutines WAVE, WAHR, GEOPRO, and REFLEX have been added to calculate the wave-slope statistics and the geometry. The subprogram TRANS is modified through the introduction of the subroutine FRESNEL (figure 5). FRESNEL calculates the reflectivity and emissivity according to equation 6.

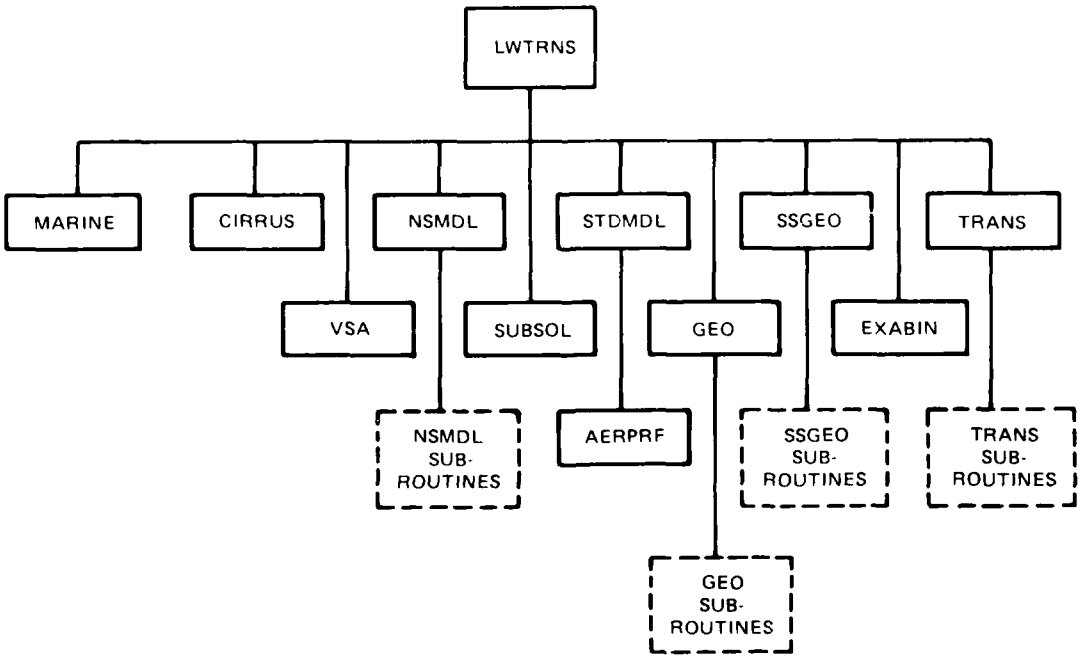

Figure 3. LOWTRAN 6 program structure.

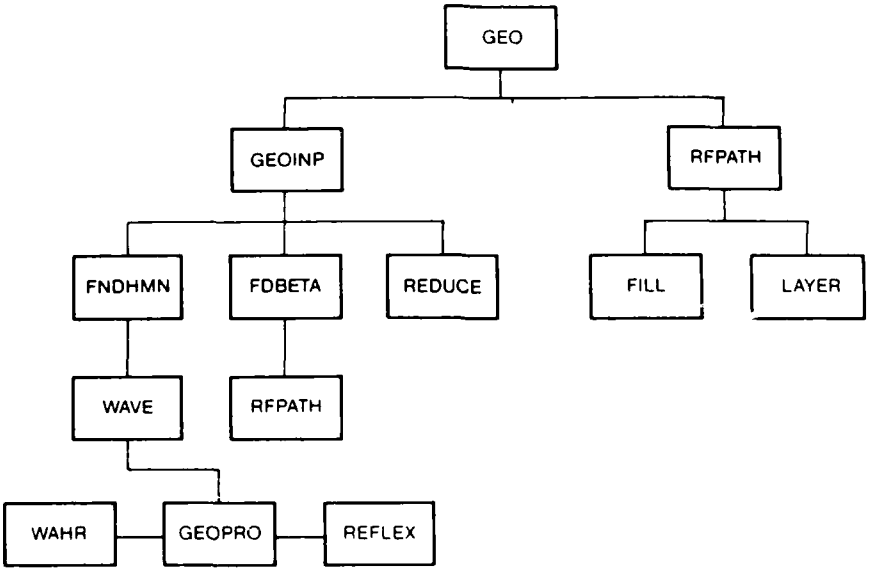

Figure 4. The structure of subprogram GEO - modified by WAVE, WAHR, GEOPRO and REFLEX.

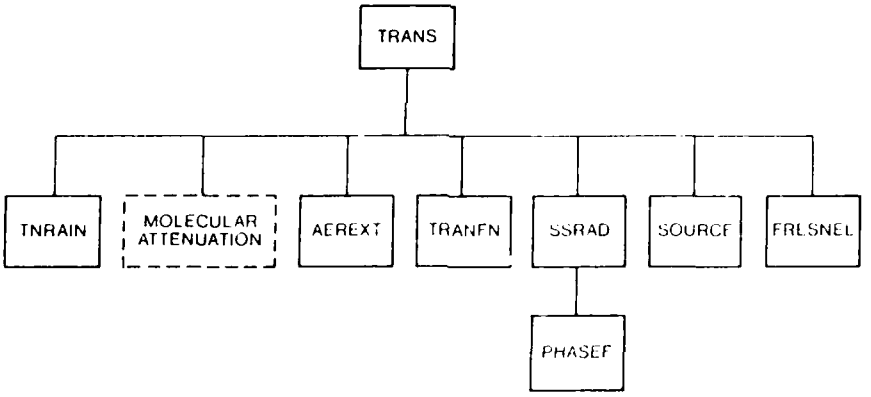

Figure 5. Subroutine FRESNEL is added to the subprogram TRANS.

3.2 PROGRAM FUNCTIONS

As few as possible changes were made within the original LOWTRAN code to allow the modified version to run in the way in which the users were accustomed.

When the subprogram FNDHMN detects that the optical path intersects the earth, the subroutine WAVE will be activated to calculate the wave-slope statistics. WAVE creates a LOWTRAN-compatible data set (file: WAVE.DAT) of zenith angles tha' allows radiance to be reflected into the line-of-sight. Thereafter, the program returns into the LOWTRAN main program to restart the calculation. The new data set will be read and the radiances will be calculated. In the subprogram TRANS, the radiances will be multiplied with the probability of

the corresponding zenith angle classes. The subroutine FRESNEL calculates the reflectivity for each wave number. After calculating the radiances for the introduced zenith angles, the result of equation (2) is calculated and the program continues at the point where it was interrupted.

To assure that all the different subroutines work together, several changes had to be made within the LOWTRAN main program and in the subroutines GEO, GEOINP, FNDHMN, and TRANS. Those changes were marked in the source code (C###..##). Two new common blocks, together with new control variables (ISEM, IDISEM, IST) were introduced. ISEM controls the process when the optical path intersects the earth. IST controls the integration of equation (2) within the subroutine TRANS.

The variables ISEM and IDISEM were introduced into the subprograms GEO and GEOINP. According to their value, the program continues the normal execution (ISEM = 0 or 1 respectively ISEM = 2 and IDISEM = 0) or it returns into the main program (ISEM = 2 and IDISEM > 0) when the optical path hits the earth. These parameters assure a coordinated program variables.

The subprogram FNDHMN detects whether the earth is hit by an optical path or not and accordingly the value of the variable ISEM is set. For ISEM = 1 (hit surface), the subroutine WAVE is called, the wave-slope statistic is calculated, and ISEM is set to 2 by WAVE.

The source code of the modified subroutines of LOWTRAN 6, together with the added subprograms can be found in Appendix 2.

4.0 EXPERIMENTAL INVESTIGATION

To verify the model, several measurements were taken to provide sea and sky radiances data together with meteorological information.

4.1 AGA MEASUREMENTS OF 8- TO 12-μm RADIANCE

The 8- to 12-μm radiance was measured with a calibrated thermal-imaging system (AGA Thermovision Model 780). The lens had a field-of-view of 2.95°, and an instantaneous field-of-view of 0.9 milliradian (mr). The system response is determined by placing a blackbody of known temperature ($\pm$ 0.1°C accuracy) in front of the system so that it filled the instantaneous field-of-view. The digitized video-signal transfer signal of the system then allows the temperature of the blackbody to be reproduced within $\pm$ 0.2°C. To measure sea and sky radiance the system was positioned pointing west towards the ocean on the Point Loma peninsula in San Diego, CA. The height was about 33 m above mean sea level.

4.2 MEASUREMENT OF METEOROLOGICAL PARAMETERS

The LOWTRAN 6 model needs vertical profiles of temperature, relative humidity, and pressure as an input to calculate the horizon and sky radiances. To measure the temperature, humidity, and pressure, two different systems were used. A Vaisala RS 80 radiosonde, used as a dropsonde, was released from a Piper Navajo aircraft. The other system was the aircraft equipped with the Rosemount temperature and pressure probes, an EG&G dewpoint sensor, and a Barnes PRT 5 radiation thermometer to measure the sea-surface temperature. After releasing the dropsonde at the 9000 foot altitude, the aircraft spiraled down to an altitude of 100 feet. Both systems gathered a temperature, humidity, and pressure profile during the descent.

Comparisons between the systems brought up questions about the accuracy of the radiosonde system. The accuracy of the pressure sensor is given with ± 0.5 hPa. The pressure height curves suggest that the accuracy might be closer to ± 1.0 hPa. The visual humidity values were especially low in clouds. As a consequence, the aircraft system was used in most cases.

4.3 AVAILABLE DATA SETS

The inaccuracy of local forecasts of fog/stratus dissolution times made it impossible to gather radiance measurements, together with aircraft/radiosonde data for more than three days. Table 1 lists the measurement days and the systems used.

Table 1. Measurement days and systems.

30 June 1987	AGA + Vaisala RS 80 + Piper Navajo
8 September 1987	AGA + Piper Navajo
17 September 1987	AGA + Piper Navajo

Figures 6, 7, and 8 show measured temperature and humidity profiles as a function of altitude.

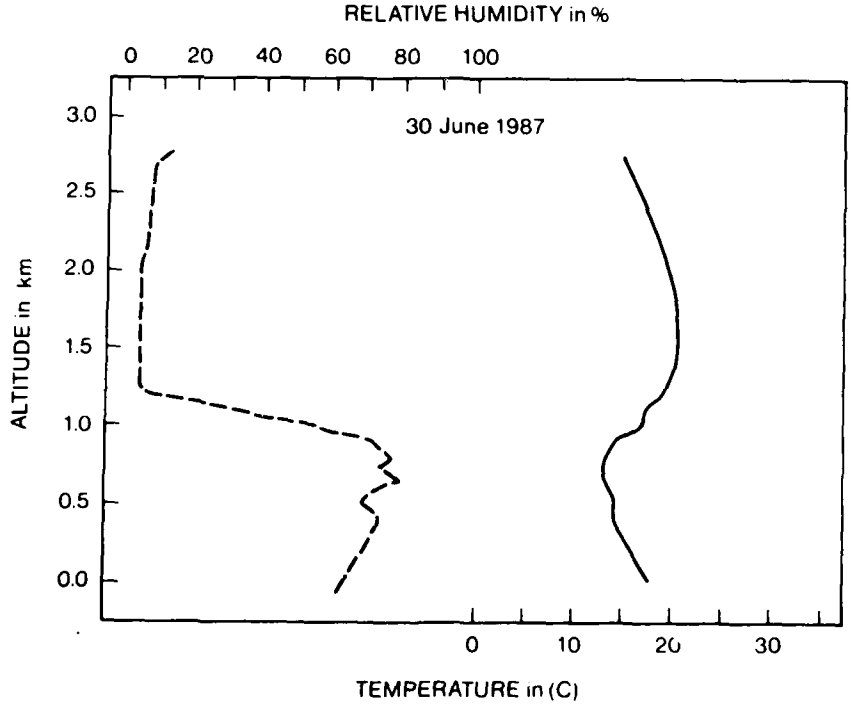

Figure 6. Soundings of temperature and relative humidity for 30 June 1987.

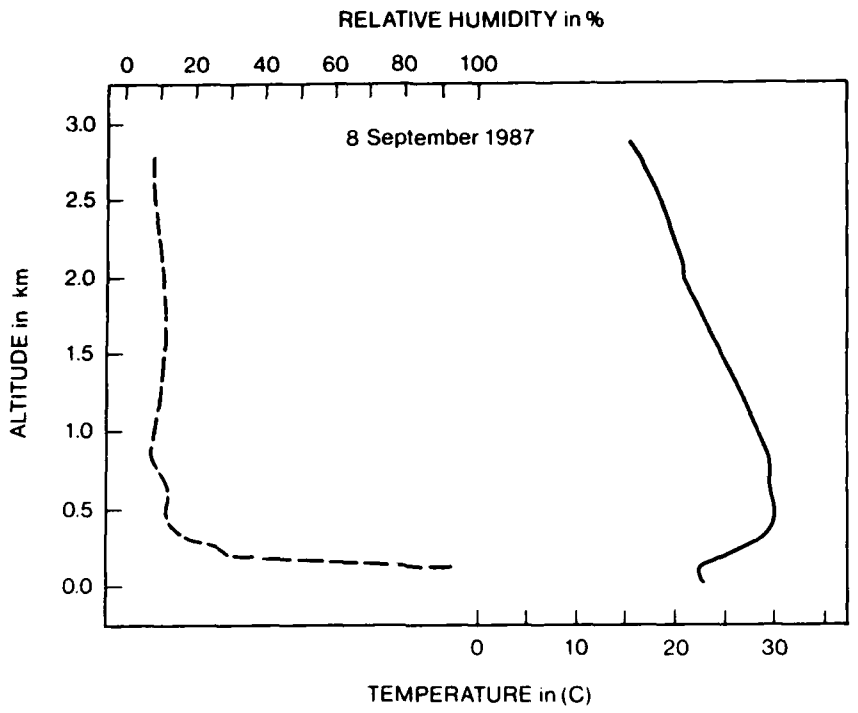

Figure 7. Soundings of temperature and relative humidity for 8 September 1987.

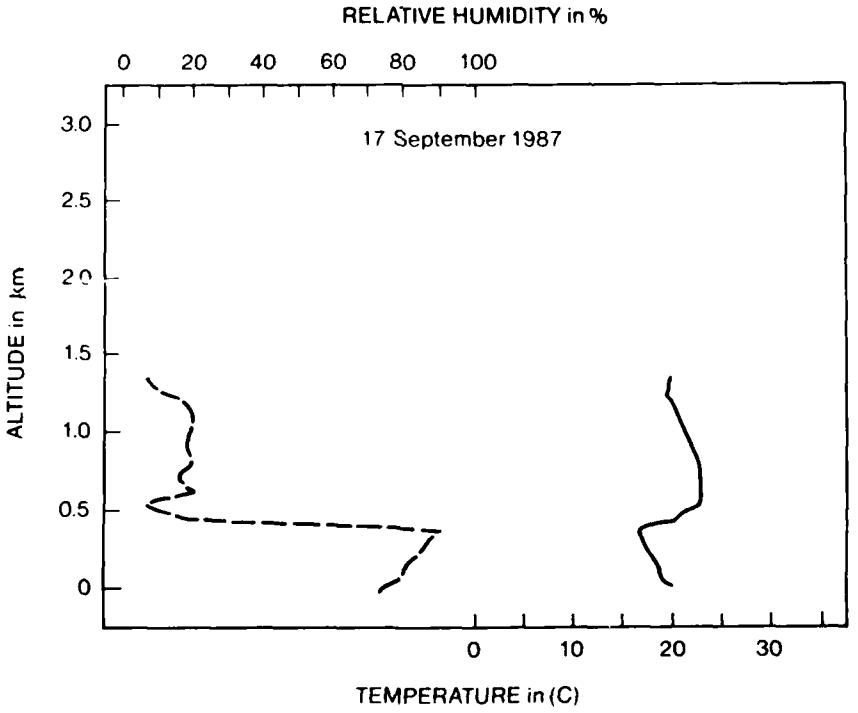

Figure 8. Soundings of temperature and relative humidity for 17 September 1987.

5.0 SIMULATION RESULTS

This paragraph presents simulation results of the model and, whenever possible, compares them with measurements of the sea and sky radiances. The zenith angles are referenced to a sensor height of 33 m above mean sea level. The measured temperature and humidity profiles were extrapolated up to 40 km using a standard atmosphere.

5.1 DEPENDENCY OF RADIANCE ON WIND VELOCITY

Figure 9 shows the radiance calculated with the meteorological data of 30 June 1987. The Maritime aerosol model was used with the visibility set to 72 km. The radiance of sea and sky is shown as a function of zenith angle for 5 different wind velocities (WS = 0.1, 1.0, 5.0, 10.0 and 20.0 m/s).

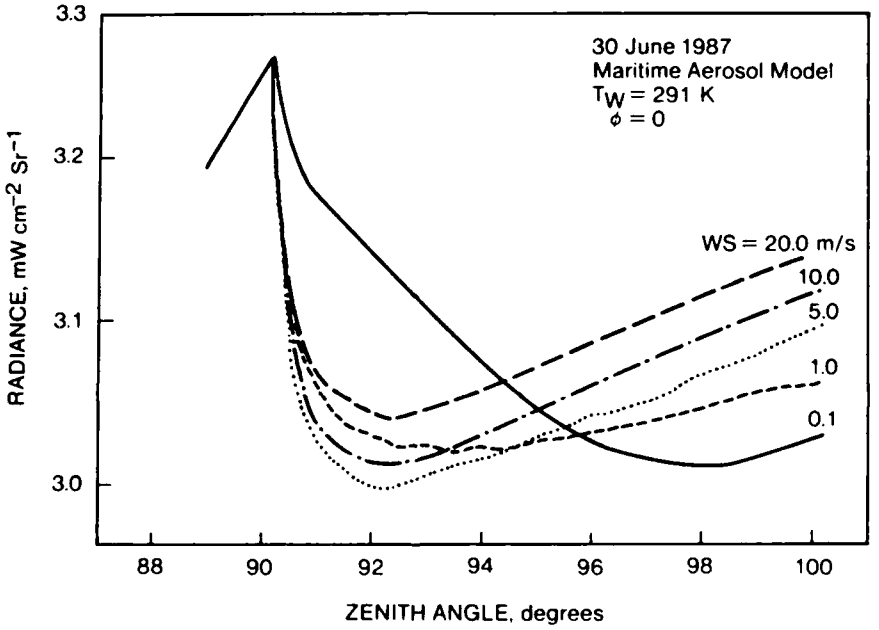

Figure 9. Radiance as a function of zenith angle and wind velocity.

A common feature of all curves is the steep decrease of radiance for zenith angles below the horizon. As the zenith angle is increased, a minimum radiance is reached. After that, the radiance rises again. This increase in radiance can be explained by the greater importance of emitted sea radiance. The behaviour of the curves in this region is determined by the water temperature and the windspeed that controls the reflectivity/emissivity. For velocities less than 1.0 m/s, the radiances just below the horizon are relatively high. The smoother sea surface reflects sky radiance just above the horizon with relatively high radiation temperature. For higher windspeeds, sky radiance from lower zenith angles (lower radiation temperature) is reflected into the line-of-sight. In cases of low windspeeds, the minimum in radiance is found at large zenith angles (98°).

5.2 INFLUENCE OF WIND AND VIEWING DIRECTION ON RADIANCE

The calculated radiance is plotted for angle differences between wind direction and sensor azimuth as a function of zenith angle (figure 10). Again, the meteorological profiles of 30 June 1987 were used together with the maritime aerosol model and a visibility of 72 km. The calculations were for two different windspeeds, 1.0 and 10.0 m/s.

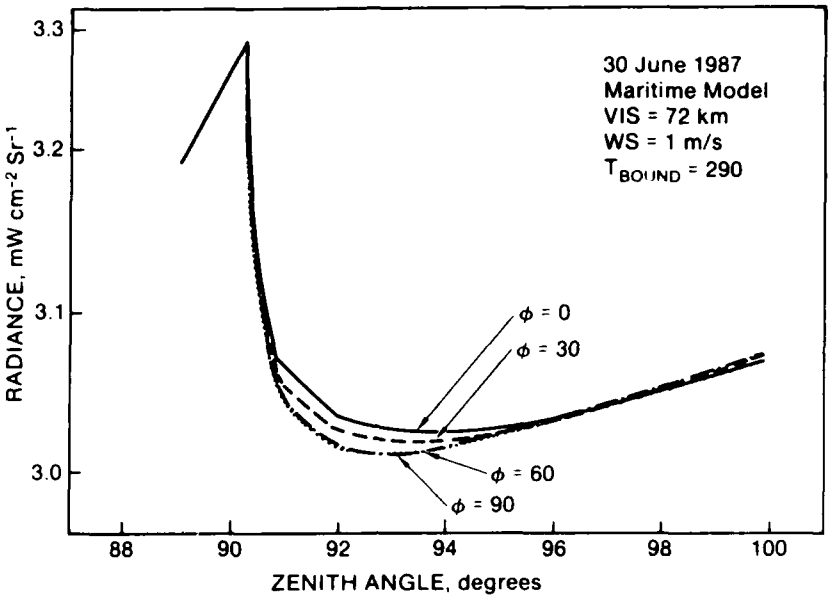

Figure 10a. The influence of wind- and viewing direction on radiance. WS = 1.0 m/s.

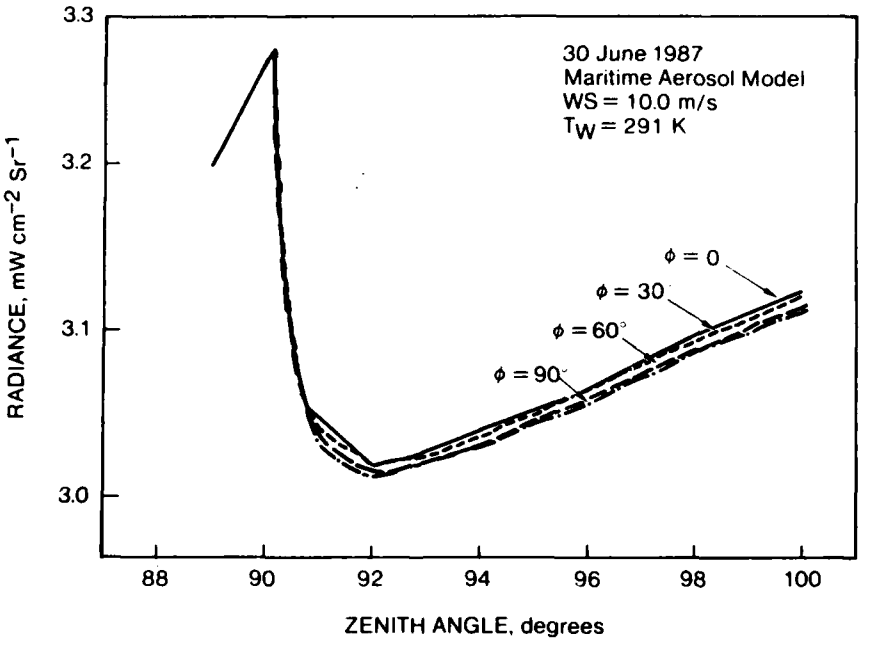

Figure 10b. The influence of wind- and viewing direction on radiance. WS = 10.0 m/s.

The radiance was not affected up to a zenith angle of about 91°. As the zenith angle increases further, the radiances differ slightly for the various angle differences. The influence of this parameter is not as important as the influence of wind velocity on radiance. The wind direction dependency may be omitted and the two dimensional gaussian distribution replaced by a one dimensional gaussian distribution.

5.3 CASE STUDIES

The radiances calculated using the meteorological data of 30 June 1987, 8 September 1987, and 17 September 1987 will be compared with the radiances measured with the AGA system. In all cases, the Navy Maritime aerosol model (Gathman, 1983) was used. The aerosol size distribution of this model is controlled by the current windspeed, the 24-hour average of the windspeed and a constant airmass (AM) factor, representing the origin of the airmass. The default value of AM in LOWTRAN 6 was used for all calculations. Wind velocities were measured at the location where the AGA system was positioned. Water temperatures were determined with the airborne PRT 5 radiation thermometer. Windspeeds and water temperatures are given in the legend to each figure.

Figure 11 shows the measured as well as the calculated radiance for 30 June 1987. The agreement between calculated and measured radiances was good. The deviations between both curves can be explained by the kelp fields that affected the measured radiances. The effects of the kelp on sea surface roughness can be visually seen. In the area of the kelp, the sea surface was smoother. Short and steep waves appeared to be damped. Aircraft measurements showed that the sea surface temperature was also affected. In the area of the kelp, and between kelp and shore the temperature was higher than in the open ocean. But even with those deviations, the agreement between measured and calculated values was surprisingly good.

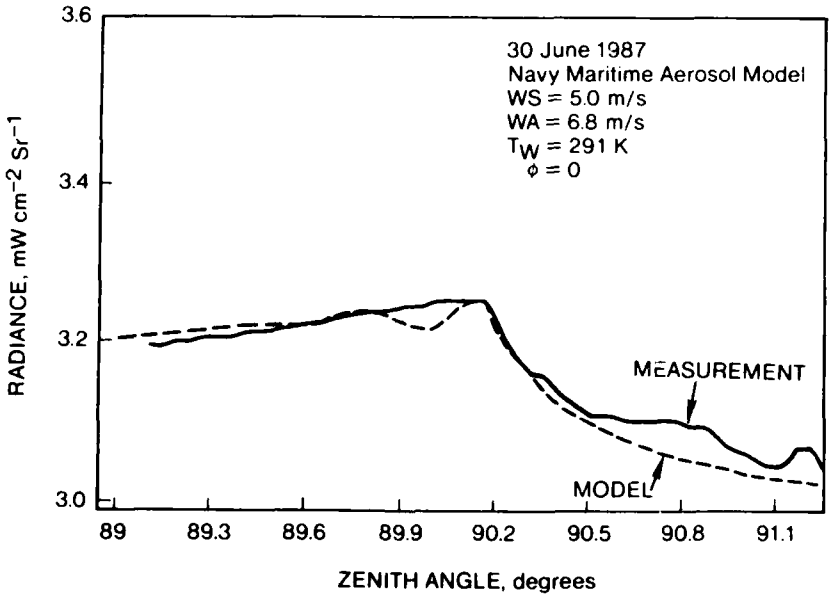

Figure 11. Comparison between measured and calculated radiances for 30 June 1987.

The data of 8 September 1987 can be compared with 30 June 1987 in respect to windspeed and water temperature. But, as figure 12 shows, the agreement between calculated and measured radiances was better on 8 September 1987. On this day, the visibility was very poor — the Coronado islands, about 30 km away, were not visible. This might have contributed to the better agreement since we expected a stronger influence of the atmosphere between sensor and sea surface and less contribution by the ocean.

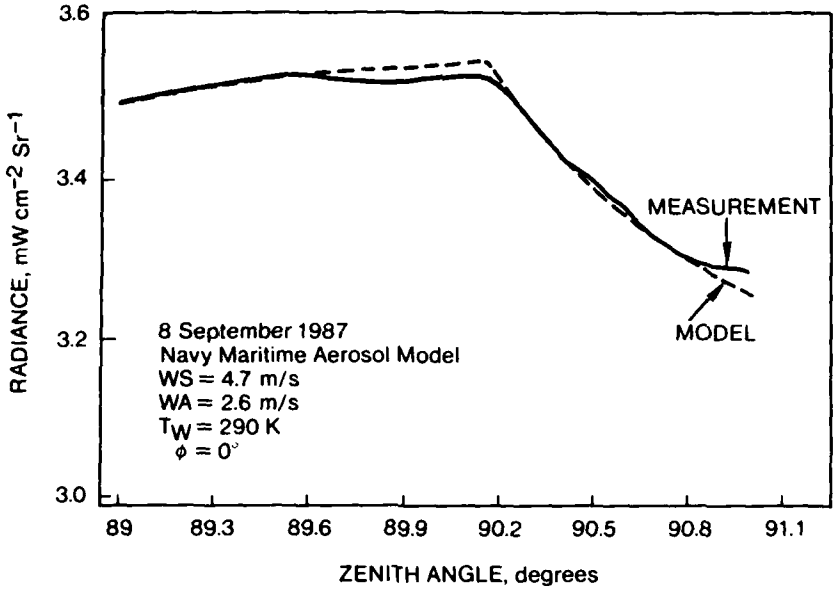

Figure 12. Measures and calculated radiances as a function of zenith angle for 8 September 1987.

The results of 17 September 1987 are presented in figure 13. This data show the largest differences between calculated and measured radiances (the differences in radiance are proportional to differences of less than 1.0°C in radiation temperature). There are several possible explanations. First of all, the temperature and humidity profiles were available only up to a height of 1.3 km whereas in the other cases the profiles reached up to 2.8 km. That affected the calculations (we do not know how much). A second possibility is that the influence of kelp fields changed with windspeed.

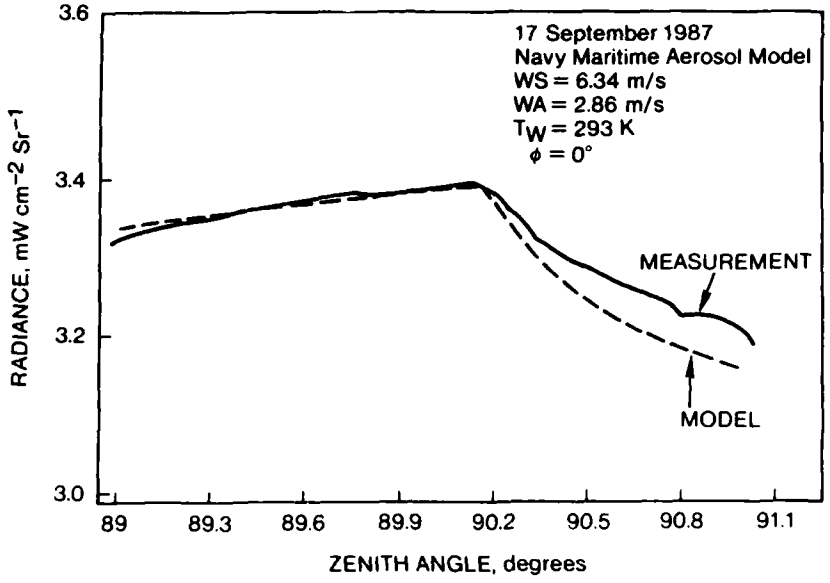

Figure 13. Measured and calculated radiances as a function of zenith angle for 17 September 1987.

6.0 CONCLUSIONS

The paper showed that the suggested sea-radiance model was able to predict sea radiances both qualitatively and quantitatively correct in three cases. Further studies should show how often a simple sea-state model can be used and under which circumstances it fails.

Further investigations should address the maximum height requirement at which the temperature and humidity profiles need to be measured to obtain better agreement between measured and calculated radiances.

The maximum number of required zenith angles representing the measured radiances needs to be determined. Also the validity of a single frequency-dependent emissivity and reflectivity needs to be investigated.

7.0 SYMBOLS AND ABBREVIATIONS

$BB(k,T_a)$	—	Planck blackbody function
EMIS	—	mean emissivity of the sea
k	—	wave number
$P(\mu)$	—	probability that radiance from the zenith angle μ reaches the sensor
$P(S_x,S_y)$	—	probability of the wave tilts S_x, S_y
P(i)	—	probability that radiance from the i-th zenith angle class reaches the sensor
P_o	—	probability for shadowing
$R(\Omega,k)$	—	reflectivity
R_1	—	reflectivity for parallel polarized waves
R_2	—	reflectivity for perpendicular polarized waves
$S(\Theta,k)$	—	radiance
$S(\Theta,k)$	—	mean radiance
S_x	—	wave tilt in x-direction = tan α
S_y	—	wave tilt in y-direction = tan β
s	—	position on the optical path
s_o	—	sensor position
s_1	—	reflector position
s_∞	—	infinity
T_a	—	air temperature
T_w	—	water temperature
α	—	angle of wave tilt in x-direction
β	—	angle of wave tilt in y-direction
Θ	—	sensor zenith angle
Θ'	—	sensor zenith angle at the reflection point modified by atmospheric refraction
μ	—	zenith angle from where radiance is reflected into the observer line of sight
$\mu(i)$	—	mean zenith angle of the i-th class
σ_x	—	standard deviation of the wave tilt S_x
σ_y	—	standard deviation of the wave tilt S_y
τ	—	total transmission = $\tau_a\tau_s$
τ_a	—	absorption transmission
τ_s	—	scattering transmission
Φ	—	angle difference between wind direction and sensor azimuth
Ω	—	reflection angle
$\Omega(i)$	—	mean reflection angle of the i-th class
IR	—	infrared
P	—	pressure
RH	—	relative humidity
WS	—	windspeed

8.0 REFERENCES

Cox, C. and W. Munk, 1954. "Measurement of Roughness of the Sea Surface from Photographs of the Sun's Glitter," *Journal of the Optical Society of America*, 44, pp. 838–850.

Gathman, S.G. 1983. " Optical Properties of the Marine Aerosol as Predicted by the Navy Aerosol Model," *Optical Engineering*, 22, pp. 57–62.

Gordon, J.I. 1969. *Directional Radiance (Luminance) of the Sea Surface*, Scripps Institution of Oceanography, Visibility Laboratory, San Diego.

Hale, G.M. and M. R. Querry. 1973. Optical Constants of Water in the 200 nm to 200 μm Wavelength Region, *Applied Optics*, 12, pp. 555–563.

Kneizys, F.X., E. P. Shettle, W.O. Gallery, J.H. Chetwynd, Jr., L.W. Abreu, J.E.A. Selby, S.A. Clough, and R.W. Fenn, 1983. *Atmospheric Transmittance/ Radiance: Computer Code LOWTRAN 6*, Hanscom AFB, MA.

Querry, M.R., W. E. Holland, R.L. Waring, L.M. Earls, and M.D. Querry. 1977. "Relative Reflectance and Complex Refractive Index in the Infrared for Saline Environmental Waters," *Journal of Geophysical Research*, 28, pp. 1425–1433.

Saunders, P.M. 1968. "Radiance of Sea and Sky in the Infrared Window" 800–1200 cm^{-1}, *Journal of the Optical Society of America*, 58, pp. 645–652.

Schwartz, I.B. and D. Hon, 1986. *Emissivity as a Function of Surface Roughness: A Computer Model*, Naval Research Laboratory, NRL Memorandum Report 5816, Washington DC.

Sidran, M. 1981. "Broadband Reflectance and Emissivity of Specular and Rough Water Surfaces," *Applied Optics*, 20, pp. 3176–3183.

Stratton, J.A. 1941. *Electromagnetic Theory*, New York, McGraw-Hill.

Wilf, I. and Y. Manor, 1984. "Simulation of Sea-Surface Images in the Infrared," *Applied Optics*, 23, pp. 3174–3180.

Wu, J. 1972. "Sea-Surface Slope and Equilibrium Wind-Wave Spectra," *Physics of Fluids*, 15, pp. 741–747.

APPENDIX A: SHADOWING OF WAVES

The shadowing of waves by other waves is a problem, especially for zenith angles close to the horizon. Other authors limit the possible zenith angle range of their models to values far away from the horizon (Sidran, 1981; Schwartz and Hon, 1986) or they omit the contributions entirely (Saunders, 1968).

In this paper, the waves are assumed to be statistically independent from one another. Under this assumption, McAdam (1969) (in the paper of Gordon, 1969) showed that the probability for shadowing depends only on the incident angle (relative to the vertical) and on the standard deviation of the wave slopes. If we assume that the wave slope distribution for the shadowing waves is also given by the Cox-Munk wave-slope statistic, the shadowing effects can be determined by the probabilities for the occurrence of the zenith angle μ.

For a given set of parameters, Θ, σx, σy, the probability for shadowing is P_o. In this case, the optical paths contained in P_o do not hit the wave facet under consideration. The optical paths hit a facet out of a normally distributed ensemble. These rays are again shadowed with P_o and so forth. When $P(\mu)$ is the probability (including shadowing) that radiance is reflected from the zenith angle μ into the line-of-sight, we have the probability $P_1(\mu) = (1 - P_o) P(\mu)$. Of the shadowed optical paths, a percentage $P_2 = P_o(1 - P_o)P(\mu)$ of radiance is reflected from the zenith angle μ into the sensor. This can be repeated.

1. shadowing $\quad P_1(\mu) = (1 - P_o)*P(\mu)$

2. shadowing $\quad P_2(\mu) = P_o*(1 - P_o)*P(\mu)$

3. shadowing $\quad P_3(\mu) = P_o^2*(1 - P_o)*P(\mu)$

.

.

n. shadowing $\quad P_n(\mu) = P_o^n*(1 - P_o)*P(\mu)$

If the single contributions are added, we get for $n \rightarrow \infty$:

$$S_n = (1 - P_o^n)P(\mu), \quad P_o < 1$$

$$\lim 1 - P_o^n = 1$$

$$S_n = P(\mu)$$

After a large number of steps, we obtain the true probability $P(\mu)$ for radiance reflected from this zenith angle. It is possible to simplify the calculation by integrating over the zenith angle after the first step to obtain

$$P(\mu) = P_1(\mu)/(1 - P_o) = P_1/\Sigma P_1 .$$